Multiphysics Modeling and Experimental Validation of the Active Reduction of Structure-Borne Noise

Tomasz G. Zielinski
Department of Intelligent Technologies,
Institute of Fundamental Technological Research,
ul. Pawinskiego 5B,
02-106 Warszawa, Poland
e-mail: tzielins@ippt.gov.pl

This paper presents a fully coupled multiphysics modeling and experimental validation of the problem of active reduction of noise generated by a thin plate under forced vibration. The plate is excited in order to generate a significant low-frequency noise, which is then reduced by actuators in the form of piezoelectric patches glued to the plate with epoxy resin in locations singled out earlier during finite element (FE) analyses. To this end, a fully coupled FE system relevant for the problem is derived. The modeling is very accurate: The piezoelectric patches are modeled according to the electromechanical theory of piezoelectricity, the layers of epoxy resin are thoroughly considered, and the acoustic-structure interaction involves modeling of a surrounding sphere of air with the nonreflective boundary conditions applied in order to simulate the conditions found in anechoic chamber. The FE simulation is compared with many experimental results. The sound pressure levels computed in points at different distances from the plate agree excellently with the noise measured in these points. Similarly, the computed voltage amplitudes of controlling signal turn out to be very good estimations.
[DOI: 10.1115/1.4001844]

Keywords: low-frequency noise reduction, multiphysics modeling, active structural acoustic control

1 Introduction

Effective noise reduction is nowadays a very important topic, since a reduced level of noise tends to be one of the crucial factors in the design of automotive vehicles and aircraft. It is true, however, that in reality, this is still a very neglected factor, on account of that in practical use are solely passive techniques for noise reduction (i.e., porous liners and screens with air-gaps.). Thus, in aircraft, noise radiated or induced by engines is often very poorly alleviated, particularly, at low frequencies. As matter of fact, inside aircraft cabins the highest sound pressure levels (SPLs) are for low-frequency noise, typically from 100 Hz to 250 Hz. Similar noise conditions are observed in vehicles.

It is obvious that in the case of aircraft and vehicles, passive means to reduce low-frequency noise are completely inefficient: To passively reduce noise at 150 Hz by 30 dB, one would require a sound insulation material with a thickness exceeding 50 cm. Therefore, the only efficient approach to deal with any low-frequency noise must be active.

The active techniques are traditionally divided into two groups [1,2]: the active noise control (ANC) and the active structural acoustic control (ASAC). The present study deals with the second approach, where the problem of noise is being alleviated at its "source," that is, the vibrations of noise radiating surfaces (plates, beams, and shells) are actively controlled in a way that reduces the generation of low-frequency noise [1,3]. The earliest works in that field were authored or co-authored by Fuller [4,5], who demonstrated through analytical and experimental investigations that the narrow band acoustic radiation from a beam can be controlled by applying the active point forces to the radiating beam.

The modeling and analysis of ASAC represent a high level of complexity, and now, there is a need for more accurate, fully coupled modeling of such problems, involving finite element, multiphysics codes. However, simplified, classical models are still in use and often prove their efficiency, especially, for problems where analytical solutions can be used. For example, Lin et al. [6] presented a numerical simulation of the problem of active control of structural acoustic pressure in a rectangular cavity with a flexible beam. The wave equation of the acoustic pressure and the equation of motion of the beam were approximated via the series expansions, and then expressed in state space form.

Another, purely numerical, harmonic-frequency simulation of active control of structural vibration and acoustic radiation of a laminated plate was given in Ref. [7]. In this work, based on the first order shear deformation theory, a finite element formulation was developed for laminated plate integrated with piezoelectric layers and viscoelastic layer. Then, the Rayleigh integral on the plate surface was coupled with the derived finite element formulation to model acoustic fluid-structure interaction of the baffled laminated plate. Even simpler and more approximative, purely analytical approach is used by Choi [8] in his paper on active structural acoustic control of a smart plate, involving well-known solutions for thin, isotropic, rectangular plates.

Carneal and Fuller [9] presented an analytical and experimental investigation of active control of sound transmission through double panel systems. They applied an approximated structural model of a baffled double panel arrangement, consisting of an incident plate and a radiating plate coupled by an air cavity, assuming also a steady-state sinusoidal response of such system.

A performance of the active constrained layer damping treatment for active structural acoustic control of laminated cylindrical panels was investigated numerically in Ref. [10], where a finite element model was developed for the laminated panels coupled with acoustic cavity. For such cavity systems, the sound pressure level was found to be attenuated up to 20 dB.

Contributed by the Technical Committee on Vibration and Sound of ASME for publication in the JOURNAL OF VIBRATION AND ACOUSTICS. Manuscript received September 17, 2009 final manuscript received April 27, 2010; published online October 8, 2010. Assoc. Editor: Thomas J. Royston.

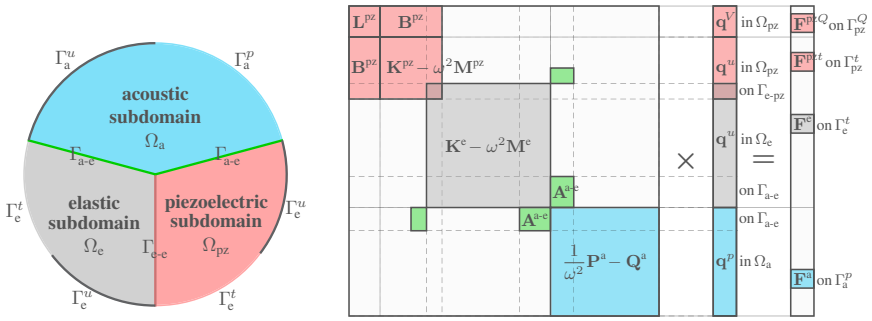

Fig. 1 Multiphysics system

In all these typical works mentioned above, active piezoelectric elements were modeled in a simplified manner. Now, an accurate, electromechanical, three-dimensional modeling of piezoelectric patches is used, for example, by Malgaca and Karagülle [11] for a simpler, classical problem of active vibration control of smart beams under harmonic excitation. That paper provides FE simulation (using ANSYS), as well as experimental verification.

A multiphysics approach to model a problem of noise transmission through active acoustic panels is applied by Galland and co-workers [12–14]. They have started to study active sandwich panels with a core of poroelastic material and piezoelectric patches glued to elastic faceplates. In these papers, the piezoelectric elements as well as the poroelastic core are modeled very accurately, using fully coupled theories; however, the influence of glue is neglected. Moreover, the results presented in Refs. [12,13] are purely numerical, while the paper by Batifol et al. [14] brings a comparison of results obtained using FE modeling with some analytical developments, showing also some findings of a preliminary experimental test. Finally, a similar, fully coupled modeling of piezoelectric patches is presented by Filipek and Wiciak in Ref. [15], where two numerical FE models based on the active and passive damping strategies for structural acoustic control of a smart beam are compared.

In the present work, a very accurate, multiphysics modeling will be applied for the ASAC problem of a plate emitting a low-frequency noise into the open air. This approach will involve the fully coupled, electromechanical theory of piezoelectricity to model piezoelectric actuators, and the acoustic-structure interaction to model how the generated noise propagates in air in the vicinity of plate (near-field). For finite element modeling COMSOL MULTIPHYSICS environment (linked with MATLAB) will be used, where the weak formulations of all involved phenomena will be implemented in the form of symbolic expressions. The modeling will be carefully validated by the experiment carried out in anechoic chamber, involving measurements of the plate's vibrations, sound pressure levels of the generated noise, and voltage amplitudes of controlling signals.

2 General Idea of the Experimental Simulation and Modeling

The experimental simulation and modeling of the problem of active reduction of structure-borne noise will consist of two successive phases. Phase 1 is solely devoted to the generation and modeling of structure-borne noise and will be called the *passive phase*. Phase 2 is the *active phase* where the feasibility and performance of active reduction are studied.

Phase 1 (passive). The main purpose of the passive phase is to simulate—experimentally and in numerical model—an unwanted behavior of a panel vibrating at low frequency. As a matter of fact, the panel will be a generic substructure—a sort of substitute for a part of structure like casing or fuselage. Moreover, the unwanted behavior must be strong enough to produce a disturbing noise. Thus, the following requirement must be satisfied: the low-frequency mode-shape of the vibrating panel should generate a *significant* noise of low-frequency. Another task to accomplish in phase 1 is a credible estimation of the structure-borne noise emitted by the panel. To this end a thorough multiphysics modeling based on the acoustics-structure interaction approach must be carried out and the results are to be validated by measurements.

Phase 2 (active). After satisfactory results are achieved in the first phase, the second phase begins, which is a proper phase to test the active approach to the reduction of structure-borne noise. The active approach means that some external energy is inputted to the system. In this case, it is the electrical energy sent to some piezoelectric actuators (fixed to the panel) where it is transformed into the mechanical energy in order to damp some noisy modes of vibration. The multiphysics modeling and experimental testing performed during the active phase are aimed to check the feasibility of active reduction of structure-borne noise and eventually allow for optimal choice of localization, size, and shape of piezoelectric actuators.

3 Multiphysics Modeling

3.1 General Assumptions and Involved Theories. As it has already been mentioned, the problem of active reduction of structure-borne noise is modeled in a very accurate way using the so-called multiphysics approach; that is, all relevant problems (different materials and phenomena) are modeled together as a one coupled system. Nevertheless, some possible simplifications and uncouplings are also taken into account (see Sec. 3.7).

The considered vibroacoustic problem allows for linear modeling because all the vibrations are small and all the coexisting media behave in a linear way. Thus, a necessary mutiphysics system combines the linear theories of acoustics, elasticity, and piezoelectricity (see Fig. 1, left), where the coupling occurs on the interfaces between different media. Moreover, the last of the involved theories describes a problem, which is by itself coupled. Since the system is linear the superposition principle holds and may be effectively used, and the frequency analysis may be used as an efficient tool for design and testing. Thus, all considered problems are time harmonic with the frequency f and the angular frequency $\omega=2\pi f$. Finally, the problems of elasticity and piezoelectricity are considered with zero body forces, which are irrelevant. Moreover, in the case of piezoelectricity there is no body electric charge applied. These assumptions comply exactly with the modeling requirements.

A complete, weak variational formulation suitable for the Galerkin finite element approximation of the harmonically driven multiphysics system shown in Fig. 1 consists of the weak formulations for individual subdomains (media) and the interface-coupling integral for acoustic-structure interaction. These weak integrals will be briefly discussed below together with some relevant boundary conditions. For the sake of brevity, symbols $d\Omega$ and $d\Gamma$ are skipped in all the integrals presented below since it is obvious whether an integration is on the specified domain or boundary. The summation convention is used (for dummy indices

i,j,k,l) and the (invariant) differentiation symbol which, in the Cartesian coordinate system, simply reads $(.)_{|i}=\partial(.)/\partial x_i$. The following notation rule applies for the symbol of variation (or test function): $\delta(vw)=v\,\delta w+w\,\delta v$, where v and w are two dependent variables (fields) and δv and δw their admissible variations.

3.2 Weak Form for an Elastic Solid. Let Ω_e be an elastic solid domain with mass density ρ_e and boundary Γ_e, and n_i^e the components of unit vector normal to the boundary and pointing outside the domain. Assuming zero body forces and the case of harmonic oscillations the weak variational form of the problem of elasticity expressing the principle of virtual work reads (for every admissible δu_i^e)

$$\mathcal{WF}_e = -\int_{\Omega_e} \sigma_{ij}^e \delta u_{i|j}^e + \int_{\Omega_e} \omega^2 \rho_e u_i^e \delta u_i^e + \int_{\Gamma_e} \sigma_{ij}^e n_j^e \delta u_i^e \tag{1}$$

where δu_i^e is the arbitral yet admissible variation of displacements; the elastic stress tensor $\sigma_{ij}^e=\sigma_{ij}^e(\mathbf{u}^e)$ substitutes here a linear function of elastic displacements $\mathbf{u}^e=\{u_i^e\}$. In the case of the linear isotropic elasticity, it can be expressed as follows:

$$\sigma_{ij}^e = \mu_e(u_{i|j}^e + u_{j|i}^e) + \lambda_e u_{k|k}^e \delta_{ij} \tag{2}$$

where the well-known Lamé coefficients, the shear modulus μ_e and the dilatational constant λ_e, appear.

For the sake of brevity, only von Neumann and Dirichlet boundary conditions for an elastic solid will be discussed here (the Robin type will be skipped). The Neumann (or natural) boundary conditions describe the case when forces $\hat{t}_i^e$ are applied on a boundary, that is,

$$\sigma_{ij}^e n_j^e = \hat{t}_i^e \ \text{ on } \ \Gamma_e^t \tag{3}$$

whereas the displacements, $\hat{u}_i^e$, are prescribed by the Dirichlet (or essential) boundary conditions

$$u_i^e = \hat{u}_i^e \ \text{ on } \ \Gamma_e^u \tag{4}$$

According to these conditions, the boundary is divided into two (directionally disjoint) parts, i.e., $\Gamma_e=\Gamma_e^t\cup\Gamma_e^u$. There is an essential difference between the two kinds of conditions. The displacement constraints form the kinematic requirements for the trial functions, u_i^e, while the imposed forces appear in the weak form; thus, the boundary integral, that is, the last of the integrals of Eq. (1), equals

$$\mathcal{B}I_e = \int_{\Gamma_e} \sigma_{ij}^e n_j^e \delta u_i^e = \int_{\Gamma_e^t} \hat{t}_i^e \delta u_i^e \tag{5}$$

Here, the property $\delta u_i^e=0$ on Γ_e^u has been used.

3.3 Weak Form of Piezoelectricity. Let Ω_{pz} be a domain of piezoelectric material, ρ_{pz} its mass density, and Γ_{pz} its boundary. The unit boundary-normal vector, n_i^{pz}, points outside the domain. The dependent variables of piezoelectric medium are the mechanical displacements, u_i^{pz}, and electric potential, V^{pz}. The case of harmonic oscillations (with the angular frequency ω) with no mechanical body forces and electric body charge is considered. Then, for arbitrary yet admissible virtual displacements, δu_i^{pz}, and virtual electric potential, δV^{pz}, the variational formulation of the piezoelectricity problem can be given as

$$\begin{aligned}\mathcal{WF}_{pz} = &-\int_{\Omega_{pz}} \sigma_{ij}^{pz} \delta u_{i|j}^{pz} + \int_{\Omega_{pz}} \omega^2 \rho_{pz} u_i^{pz} \delta u_i^{pz} + \int_{\Gamma_{pz}} \sigma_{ij}^{pz} n_j^{pz} \delta u_i^{pz} \\ &- \int_{\Omega_{pz}} D_i^{pz} \delta V_{|i}^{pz} + \int_{\Gamma_{pz}} D_i^{pz} n_i^{pz} \delta V^{pz}\end{aligned} \tag{6}$$

where $\sigma_{ij}^{pz}=\sigma_{ij}^{pz}(\mathbf{u}^{pz},V^{pz})$ and $D_i^{pz}=D_i^{pz}(\mathbf{u}^{pz},V^{pz})$ are expressions of mechanical displacements and electric potential. Obviously, from the physical point of view they represent the mechanical stress tensor and the electric displacement vector, respectively. As a matter of fact, these expressions are the so-called *stress-charge form* of the constitutive relations of piezoelectricity—they are given below for the case of linear anisotropic piezoelectricity:

$$\sigma_{ij}^{pz} = C_{ijkl}^{pz} \frac{u_{k|l}^{pz} + u_{l|k}^{pz}}{2} - e_{kij}^{pz} V_{|k}^{pz}, \quad D_i^{pz} = e_{ikl}^{pz} \frac{u_{k|l}^{pz} + u_{l|k}^{pz}}{2} + \varepsilon_{ik}^{pz} V_{|k}^{pz}. \tag{7}$$

Here, C_{ijkl}^{pz}, e_{ikl}^{pz}, and ε_{ik}^{pz} denote (the components of) the fourth-order tensor of elastic material constants, the third- order tensor of piezoelectric material constants, and the second-order tensor of dielectric material constants, respectively. These three tensors of material constants characterize completely any piezoelectric material, i.e., its elastic, piezoelectric, and dielectric properties. One should notice that the (linear) kinematic relations, $\varepsilon_{ij}^{pz}=(u_{k|l}^{pz}+u_{k|l}^{pz})/2$, linking mechanical strain (ε_{ij}^{pz}) and displacements (u_i^{pz}), and Maxwell's law for electrostatics, $E_i^{pz}=-V_{|i}^{pz}$, relating the electric field (E_i^{pz}) with its potential (V^{pz}), have been explicitly used in Eq. (7). The constitutive equations (7) are given for a general case of anisotropic piezoelectricity. However, piezoelectric materials are usually treated as orthotropic or even transversally isotropic.

In piezoelectricity, the boundary conditions are divided into two groups—there are mechanical conditions (referring to the elasticity problem) and electrical conditions (referring to the electricity). Consequently, the boundary of piezoelectric domain can be subdivided as follows: $\Gamma_{pz}=\Gamma_{pz}^t\cup\Gamma_{pz}^u$ and $\Gamma_{pz}=\Gamma_{pz}^Q\cup\Gamma_{pz}^V$. The parts belonging to the same group of subdivision are disjoint and both subdivisions are completely independent. Here, Γ_{pz}^t and Γ_{pz}^Q pertain to the Neumann conditions for surface-applied mechanical forces and electric charge, respectively, while Γ_{pz}^u and Γ_{pz}^V refer to the Dirichlet conditions on imposed mechanical displacements and electric potential, respectively.

Only electrical boundary conditions will be discussed here, since the mechanical ones are uncoupled, and they are identical with the conditions for an elastic solid discussed above. The electric boundary condition of the Neumann kind serves for a surface electric charge $\hat{Q}^{pz}$ applied on a boundary

$$-D_i^{pz} n_i^{pz} = \hat{Q}^{pz} \ \text{ on } \ \Gamma_{pz}^Q \tag{8}$$

whereas the Dirichlet condition allows to prescribe the electric potential $\hat{V}^{pz}$ on a boundary

$$V^{pz} = \hat{V}^{pz} \ \text{ on } \ \Gamma_{pz}^V \tag{9}$$

The electric boundary integral, that is, the last term in Eq. (6), equals

$$\mathcal{B}I_{pz}^{elec} = \int_{\Gamma_{pz}} D_i^{pz} n_i^{pz} \delta V^{pz} = -\int_{\Gamma_{pz}^Q} \hat{Q}^{pz} \delta V^{pz} \tag{10}$$

Here, the Neumann condition for electric charge (8) has been used together with the condition for voltage variation, $\delta V^{pz}=0$ on Γ_{pz}^V.

3.4 Weak Form for an Acoustic Fluid. Let Ω_a be a domain of acoustic medium (e.g., inviscid, elastic fluid) and Γ_a its boundary with n_i^a being the components of unit normal vector pointing outside the domain. Very convenient dependent variable of acoustical medium is the acoustic pressure, p^a. Now, for harmonic motion with the angular frequency ω, the following weak form can be used:

$$\mathcal{WF}_{\mathrm{a}} = -\int_{\Omega_{\mathrm{a}}} \frac{1}{\omega^2 \rho_{\mathrm{a}}} p^{\mathrm{a}}_{|i} \delta p^{\mathrm{a}}_{|i} + \int_{\Omega_{\mathrm{a}}} \frac{1}{K_{\mathrm{a}}} p^{\mathrm{a}} \delta p^{\mathrm{a}} + \int_{\Gamma_{\mathrm{a}}} \frac{1}{\omega^2 \rho_{\mathrm{a}}} p^{\mathrm{a}}_{|i} n^{\mathrm{a}}_i \delta p^{\mathrm{a}} \tag{11}$$

where ρ_{a} and K_{a} are the mass density and the bulk modulus of acoustic medium, respectively. In the case of fluids, usually, the given data are how fast a sound wave propagates in the medium. Therefore, the bulk modulus can always be replaced by $K_{\mathrm{a}} = \rho_{\mathrm{a}} c_{\mathrm{a}}^2$, where c_{a} is the speed of sound. Knowing the acoustic pressure, one can always determine the (complex amplitudes of) displacements, velocities, and accelerations of fluid particle using the following formulas:

$$u^{\mathrm{a}}_i = \frac{1}{\omega^2 \rho_{\mathrm{a}}} p^{\mathrm{a}}_{|i}, \quad v^{\mathrm{a}}_i = j\omega u^{\mathrm{a}}_i = -\frac{1}{j\omega \rho_{\mathrm{a}}} p^{\mathrm{a}}_{|i}, \quad \mathrm{a}^{\mathrm{a}}_i = -\omega^2 u^{\mathrm{a}}_i = -\frac{1}{\rho_{\mathrm{a}}} p^{\mathrm{a}}_{|i} \tag{12}$$

Two kinds of boundary conditions will be considered: the Neumann condition when a rigid piston of known accelaration, $\hat{a}^{\mathrm{a}}_i$, is imposed on a boundary, and the Dirichlet condition when a value of acoustic pressure, $\hat{p}^{\mathrm{a}}$, is prescribed. In the harmonic case: $\hat{a}^{\mathrm{a}}_i = -\omega^2 \hat{u}^{\mathrm{a}}_i$ with $\hat{u}^{\mathrm{a}}_i$ being the (complex) amplitude of displacements, and the Neumann condition reads

$$\frac{1}{\omega^2 \rho_{\mathrm{a}}} p^{\mathrm{a}}_{|i} = \hat{u}^{\mathrm{a}}_i \ \text{ on } \ \Gamma^u_{\mathrm{a}} \tag{13}$$

The Dirichlet boundary condition simply states that

$$p^{\mathrm{a}} = \hat{p}^{\mathrm{a}} \ \text{ on } \ \Gamma^p_{\mathrm{a}} \tag{14}$$

Now, using the Neumann condition (13) and the condition for pressure variation, $\delta p^{\mathrm{a}} = 0$ on Γ^p_{a}, the boundary integral, that is, the last term in Eq. (11), can be written as follows:

$$\mathcal{B}I_{\mathrm{a}} = \int_{\Gamma_{\mathrm{a}}} \frac{1}{\omega^2 \rho_{\mathrm{a}}} p^{\mathrm{a}}_{|i} n^{\mathrm{a}}_i \delta p^{\mathrm{a}} = \int_{\Gamma^u_{\mathrm{a}}} u^{\mathrm{a}}_i n^{\mathrm{a}}_i \delta p^{\mathrm{a}} \tag{15}$$

3.5 Acoustic-Elastic Coupling. The coupling integral on an interface $\Gamma_{\mathrm{a\text{-}e}}$ between elastic and acoustic subdomains is responsible for the acoustic-structure interaction; it reads as follows:

$$\mathcal{C}I_{\mathrm{a\text{-}e}} = \int_{\Gamma_{\mathrm{a\text{-}e}}} \frac{1}{\omega^2 \rho_{\mathrm{a}}} p^{\mathrm{a}}_{|i} n^{\mathrm{a}}_i \delta p^{\mathrm{a}} + \int_{\Gamma_{\mathrm{a\text{-}e}}} \sigma^{\mathrm{e}}_{ij} n^{\mathrm{e}}_j \delta u^{\mathrm{e}}_i \tag{16}$$

On the interface, the conditions of continuity of the displacements normal to the interface and normal stresses must be satisfied, that is,

$$\frac{1}{\omega^2 \rho_{\mathrm{a}}} p^{\mathrm{a}}_{|i} n^{\mathrm{a}}_i = u^{\mathrm{e}}_i n^{\mathrm{a}}_i, \quad \sigma^{\mathrm{e}}_{ij} n^{\mathrm{e}}_j = -p^{\mathrm{a}} n^{\mathrm{e}}_i \tag{17}$$

These conditions are used for the integral and since on the interface the two unit normal vectors are in the opposite direction one to another, i.e., $n^{\mathrm{a}}_i = -n^{\mathrm{e}}_i$, the interface-coupling integral (16) simplifies to

$$\mathcal{C}I_{\mathrm{a\text{-}e}} = \int_{\Gamma_{\mathrm{a\text{-}e}}} (p^{\mathrm{a}} n^{\mathrm{a}}_i \delta u^{\mathrm{e}}_i + u^{\mathrm{e}}_i n^{\mathrm{a}}_i \delta p^{\mathrm{a}}) = \int_{\Gamma_{\mathrm{a\text{-}e}}} \delta(p^{\mathrm{a}} u^{\mathrm{e}}_i n^{\mathrm{a}}_i) \tag{18}$$

Obviously, this result is also valid and, moreover, complete in the case of a piezoelectric medium in contact with an acoustic one, since the interface coupling occurs explicitly only between the acoustic problem and its mechanical (i.e., elastic) counterpart in the piezoelectric subdomain. To be formal, one should only change $\Gamma_{\mathrm{a\text{-}e}}$ to $\Gamma_{\mathrm{a\text{-}pz}}$, and u^{e}_i to u^{pz}_i in the formulas given above.

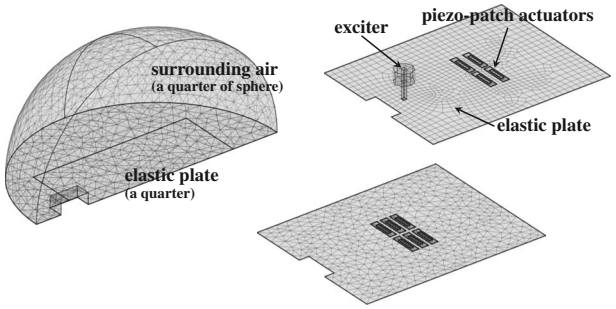

Fig. 2 Problem geometries and FE meshes

3.6 Weak Formulation for Galerkin Finite-Element Approximation. The coupled multiphysics model of a harmonic system made up of acoustic, elastic, and piezoelectric media (see Fig. 1) was constructed, according to the Galerkin approximation method, using the following weak integral:

$$\mathcal{WF}_{\mathrm{e}} + \mathcal{WF}_{\mathrm{pz}} + \mathcal{WF}_{\mathrm{a}} + \mathcal{C}I_{\mathrm{a\text{-}e}} = 0 \tag{19}$$

where $\mathcal{WF}_{\mathrm{e}}$, $\mathcal{WF}_{\mathrm{pz}}$, and $\mathcal{WF}_{\mathrm{a}}$ are the weak forms of linear elasticity, Eq. (1), piezoelectricity, Eq. (6), and acoustics, Eq. (11), respectively, whereas $\mathcal{C}I_{\mathrm{a\text{-}e}}$ is the coupling integral (16) or (18), on the interface $\Gamma_{\mathrm{a\text{-}e}}$ between the acoustic and elastic subdomains (here, the term "elastic subdomains" includes also piezoelectric one). The obtained system of algebraic equations is shown in Fig. 1 (right) as a generic discrete system with optimized ordering of degrees-of-freedom, where particular submatrices and subvectors are visualized. There are the stiffness and mass matrices for elastic solids and for piezoelectric media, respectively, $\mathbf{K}^{\mathrm{e}}$ and $\mathbf{M}^{\mathrm{e}}$, and $\mathbf{K}^{\mathrm{pz}}$ and $\mathbf{M}^{\mathrm{pz}}$. In the case of piezoelectric subdomain, there is also the electric permittivity matrix $\mathbf{L}^{\mathrm{pz}}$, and the piezoelectricity matrix $\mathbf{B}^{\mathrm{pz}}$ responsible for electromechanical coupling. There are two component matrices in the case of the acoustic subdomain matrix, namely, the kinetic energy matrix $\mathbf{P}^{\mathrm{a}}$ and $\mathbf{Q}^{\mathrm{a}}$ the compressional energy matrix. The acoustic-structure interaction is realized by the interface-coupling matrix $\mathbf{A}^{\mathrm{a\text{-}e}}$, which couples relevant degrees-of-freedom of mechanical displacements (of elastic or piezoelectric solids) and acoustic pressure (of acoustic fluid). Finally, $\mathbf{q}^u$, $\mathbf{q}^p$, and $\mathbf{q}^V$ are subvectors of the degrees-of-freedom vector $\mathbf{q}$, corresponding to the mechanical displacements, acoustic pressure, and electric potential, respectively, whereas $\mathbf{F}^{\mathrm{e}}$, $\mathbf{F}^{\mathrm{pz}Q}$, $\mathbf{F}^{\mathrm{pz}I}$, and $\mathbf{F}^{\mathrm{a}}$ are the component vectors of the right-hand-side vector resulting from the surface traction (on some boundaries of elastic and piezoelectric media), surface electric charge (on some boundaries of piezoelectric media), and acceleration (on some boundaries of acoustic media).

3.7 Actual Finite Element Modeling. Now, the modeling of actual components of the considered active vibroacoustic problem will be discussed. The thin, elastic plate is modeled using the finite element method based on the displacement formulation of linear elasticity. The elastodynamic behavior of the plate can be affected by the presence of piezoelectric exciter and patches, as well as by the surrounding air (see Fig. 2). The plate is clamped at one end and the piezoelectric patches are fixed to its upper surface so by stretching they bend the plate. To grasp this effect directly, the thin plate is modeled as three-dimensional structure.

A spherical region of air surrounding the panel is modeled using the classical pressure formulation of linear acoustics. The acoustic wave propagating in this region results from the vibrations of aluminum plate. Eventually, only a quarter of the sphere can be modeled (see Fig. 2, left) in the case of harmonic oscillations because the most relevant case of "noisy" vibrations are linked with symmetrical mode shapes. The region of surrounding air is modeled with finite elements: some distance from the plate, nonreflective boundary condition is applied in the form of the

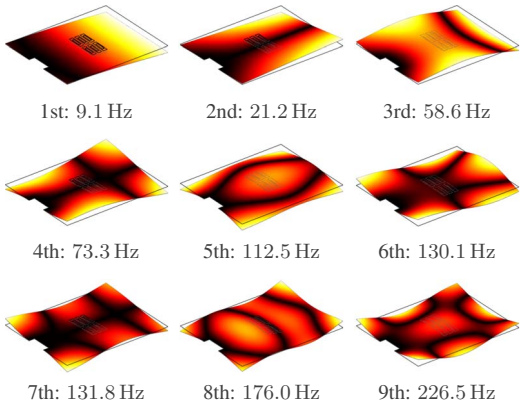

Eigenfrequencies [Hz]

No.	Measured	Calculated (with different meshes)			
1	9.1	10.45	10.49	9.98	9.83
2	21.2	26.62	26.46	25.18	24.51
3	58.6	62.81	62.15	59.08	58.00
4	73.3	87.61	85.96	82.22	80.30
5	112.5	114.11	112.84	110.65	109.36
6	130.1	132.87	131.58	127.21	125.40
7	131.8	157.52	156.07	149.07	146.58
8	176.0	220.37	210.34	203.63	200.86
9	226.5	235.80	233.92	225.03	221.89

Mesh refinement:	Normal	Fine	Finer	Finest
DOF:	18993	25554	34962	69882
elements:	1110	1507	2019	4071
mesh points:	992	1324	1856	3706

Fig. 3 Eigenmodes and eigenfrequencies

acoustic impedance of air. On other boundaries, the relevant boundary conditions are specified: the so-called no penetration condition (by setting the normal displacements of fluid particle to zero) on the rigid walls of the vice clamping the plate and on the (vertical) plane of symmetry, and the zero-pressure condition on the (horizontal) plane of antisymmetry.

Active piezoelectric elements of panel are (see Fig. 2, right): piezopatch actuators and an amplified piezoelectric exciter. To model these elements, two approaches are used, namely, (1) an accurate (three-dimensional), fully coupled theory of piezoelectricity is used in the case of piezopatch actuators, and (2) the so-called *thermoelastic-analogy approach* (which uses anisotropic elasticity with thermal loads or initial strains) is applied for the exciter. The thermal analogy is based on the resemblance between thermoelastic and converse piezoelectric constitutive equations. In this approach, the electric field is uncoupled (independent) from the field of deformation but its effect on the deformation field (i.e., the converse piezoelectric effect) can be approximated by initial (or induced actuation) strain tensor components, which are often computed as thermal strains using this analogy [16].

The multiphysics modeling involves two main types of coupling, namely, (1) the acoustics-structure interaction—in modeling of the noise generated by the vibrating elastic panel (and also to consider the impeding effect of the surrounding air), and (2) the electromechanical coupling—in modeling of the piezoelectric actuators. The acoustics-structure interaction couples the particle velocities of air in the direction normal to the surface of plate to the normal displacements (velocities) of the elastic plate. The electromechanical coupling allows to fully consider the effect of voltage drop or increase on the electrodes of piezopatch actuators caused by the actual vibrations of plate, and thus, for better estimation of the voltage amplitude of the active reduction signal that should be sent to piezopatch actuators.

As a matter of fact, to reduce the numerical model of the problem the two couplings can be taken into account separately: First, the noise (in the passive phase) can be estimated using the acoustics-structure interaction of the elastic plate (with no piezoelectric elements) immersed in the acoustic medium of air (see Fig. 2, left), and then the active approach can be tested for the plate with piezopatches (see Fig. 2, right). The result of the actively reduced vibrations can be extrapolated for the noise reduction effect. This is, in fact, a slightly simplified approach, which uncouples the passive and active phase. Nevertheless, the results obtained in that way are valid and the estimations (though less accurate) are useful.

Furthermore, the following right-handed system of reference is used for coordinates: The point of origin (0,0,0) is set in the center of the clamped edge of plate (so, in fact, it is situated inside the region of vice), the x-axis is along the length of plate (in the direction of its free edge), the y-axis is along the clamped edge, and the z-axis is perpendicular to the plate.

COMSOL MULTIPHYSICS environment (linked with MATLAB) was used to solve the problem by the finite element method. All relevant phenomena, that is, elasticity, piezoelectricity, and acoustics were implemented in this environment in the form of weak formulations (1), (6), and (11). To this end, the so-called *Weak Form, Subdomain, PDE Mode* was used for each subdomain, where all relevant formulas discussed in Secs. 3.2–3.5 were implemented as symbolic expressions. This is advanced, the most fundamental, and laborious but at the same time the most flexible and conscious approach (instead of using some dedicated *Application Modes*, which were only used for verification). The couplings were realized as explained above, refined meshes were constructed, and appropriate shape functions were chosen as discussed below.

Piezoelectric patches were modeled by hexahedral elements with the second-order (quadratic) Lagrange polynomials as shape functions for all the three component fields of displacement as well as for the scalar field of electric potential. It is important to emphasize that the usage of the second-order polynomial for the electric potential is quite important for accurate estimation of voltage amplitudes used in active control. A first order interpolation would result in a linear through-thickness variation of the electric potential and that would neglect the induced potential and the electromechanical coupling would be partial [16]. (In fact, it was shown that the asymptotic electric potential of a short circuited thin piezoelectric plate is actually quadratic in thickness [16].)

The plate, as well as some aluminum tiles and epoxy layers (see Sec. 4 below) were modeled using hexahedral elements with quadratic shape functions applied for displacement fields (see, for example, Fig. 2). In the case of the acoustics-structure interaction problem, parallelepiped elements with triangular base were used for the plate in order to merge their nodes with appropriate interface nodes of tetrahedral elements used for the acoustic medium (see Fig. 2). Again, quadratic Lagrange polynomials were used for the displacement fields and also for the field of acoustic pressure. The solutions for both types of meshing of the plate were checked and proved to be the same for the relevant low-frequency symmetric mode of interest (see Fig. 8). Obviously, the convergence in acoustic medium was excellent since for the chosen frequency of 115 Hz, the wavelength in air is almost 3 m, which is many times more than the characteristic length of even the biggest of the used tetrahedral elements. In fact, the proposed model could be used for frequencies higher than the chosen one.

The mesh convergence and modeling were tested and proved to be very good for the frequencies of interests. (To this end, among other tests, also FE and analytical solutions of a simply supported and clamped plates of the same dimensions as the one used in the study were investigated.) Still, the most important test was the consistency between the experimental and calculated results for the chosen "noisy" frequency of 115 Hz. Figure 3 presents the

Fig. 4 Experimental stand for the experiment in anechoic chamber

measured eigenfrequencies for the first nine eiegenmodes of the plate with six passive (shunted) piezopatches compared with the computed results obtained for different prismatic meshes, which can be easily merged with tetrahedral elements of the acoustic subdomain of surrounding air. (The eigenmode shapes were also confirmed experimentally by finding the lines of zero vibration velocity.) For most of the eigenmodes of symmetrical shape, the consistency between the computed and measured results was rather good. Some discrepancies were observed especially for antisymmetric modes, and also for the first and eighth modes, where the damping effect of the exciter cannot be neglected (for the eighth mode, for example, a node occurs not far from the comparatively heavy exciter). The exciter was deliberately fixed very close to the clamped area so that its mass and, especially, the fixation—which is extremely difficult to model—could be neglected (see Sec. 4.3 for more explanation). Of the uttermost importance is a very good experiment versus model consistency around the fifth and ninth modes, which are the desirable for the study low-frequency "noisy" modes (which was also confirmed experimentally).

4 Demonstration Experiment

4.1 Experimental Stand for Demonstration Experiment. Figure 4 shows the experimental stand, which was used for the demonstration experiment carried out in an anechoic chamber. The main part of the stand is a simple generic panel, or rather, as a matter of fact, an elastic faceplate of panel to which some active elements are fixed. The plate is made up of aluminum and the active elements are a few piezoelectric patches glued to its surface by the epoxy resin, and the amplified piezoelectric exciter fixed close to the clamped area.

The exciter is aimed to induce low-frequency vibrations of the plate and so it is connected to a signal generator. The vibrations of plate can be measured by a laser vibrometer, which registers the velocities of deflection at a chosen point. The vibrating plate generates an acoustic wave, which propagates in the surrounding air and can be measured by a microphone placed at some distance (typically several centimeters) behind the plate (so it is invisible on the photograph presented in Fig. 4). All the signals—generated or produced at measurements—are observed on an oscilloscope.

Eventually, an electric signal is sent to the electrodes of the piezopatch actuators so they expand and contract, thus affecting the vibrations of plate by locally induced bending. The electric signal is produced by the signal generator: In fact, it is supposed to be the same harmonic signal sent to the exciter but transformed by a signal changer.

4.2 Aluminum Plate: A Dipole Source of Low-Frequency Noise. Figure 5 presents a generic elastic faceplate of active panel. The geometrical properties of aluminum plate are as follows: the thickness is 0.93 mm, the in-plane dimensions are 280 $\times$ 224 mm^2, and the dimensions of clamped area are 52 $\times$ 15 mm^2.

As mentioned above, the first purpose of simulation is to excite the plate in order to get the greatest low-frequency acoustic response. In that way, an unnecessary behavior of a panel, which transmits/generates a low-frequency noise should be simulated. The low-frequency limit is (quite arbitrary) set to 300 Hz. It is supposed that above this frequency, passive means of acoustic insulation are sufficiently efficient and feasible (that is, involve insulating layers of acceptably moderate thickness).

Now, it is found experimentally (by sweeping through the frequency of harmonic signal sent to the exciter) that for the plate only two "noisy" modes exist at low frequencies (that is, below 300 Hz), as follows:

- approximately 113 Hz—a "loud-speaker" mode
- approximately 227 Hz—another noisy low-frequency mode

These eigenfrequencies were a few Hertz lower when no piezopatches were glued to the plate. Around each of these eigenfrequencies, a comparatively large noise is produced, which freely propagates farther from the plate surfaces. Both eigenfrequencies are confirmed by numerical frequency analyses where the corresponding mode shapes are also found—see Fig. 6 and also the photograph in Fig. 5 where the points of zero vibration velocity

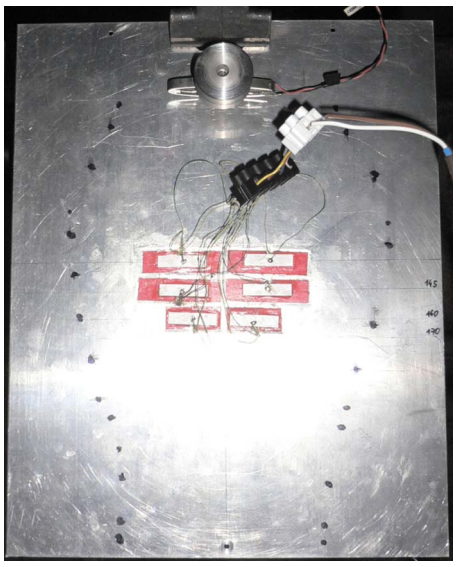

Fig. 5 Thin plate

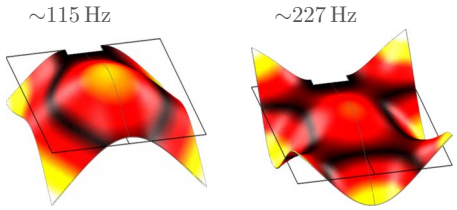

Fig. 6 Noisy low-frequency vibrations

are marked in black. One should notice that the both modes are symmetric. Although some other eigenfrequencies exist in the considered range, their eigenmodes do not produce noise because either they are below the hearing threshold of 20 Hz or they tend to be antisymmetric so that the relevant parts of plate form counteracting dipole sources of acoustic waves (the neighboring sources work in antiphase and the generated waves are mutually canceled at a short distant from the plate). For further investigations, the frequency of 115 Hz is chosen, as the one which produces stable vibrations of the shape presented in Fig. 6(left) and generates a distinct low-frequency noise.

The shapes of the "noisy" and other modes are also confirmed experimentally by manual laser scanning of the plate surface (vibrating in the particular low-frequency mode) in order to find points where the deflection velocities have zero amplitude: the marked points (visible in Fig. 5) form the neutral curves of deflection. The points of the (locally) biggest deflections can also be found by scanning and conform with the numerically obtained mode shapes.

4.3 Low-Frequency Exciter and Its Modeling. In order to simulate an unwanted behavior of a panel transmitting a low-frequency noise, the generic faceplate of panel is excited at low-frequency inducing a noisy symmetric mode. To this end, the vibration exciter (see Fig. 7) is used. It consists of the following:

- an amplified piezoelectric actuator APA100M (mass: 19.5 g, "quasistatic" stiffness: 1.67 $\mathrm{N}/\mu\mathrm{m}$) mounted on the plate at the point $(x=40\ \mathrm{mm}, y=0\ \mathrm{mm})$
- a steel weight (mass: 86 g) fixed to the free end of the APA

The aim of the steel weight is to increase the effect of the actuator so that the vibrations and consistently the generated noise are bigger.

The exciter was deliberately located closely to the clamped area. There are two reasons behind it. First, the subject of the study is the acoustics-structure interaction and the active vibroacoustic control of a plate, which can be a part of a panel driven into noisy vibrations by any cause; therefore, the presence of exciter (that is, mainly its mass) should not very much affect the structural behavior of the plate. Second, such a localization of the exciter justifies a simplified approach to its modeling; in particular, its effect may be simply modeled by a concentrated force, but even in the case of a more advanced modeling any model errors should be less influential (as a matter of fact, it appeared that the most important problem in the exciter modeling was the joint fixing the exciter to the plate). Nevertheless, two approaches for modeling the effect of the harmonically driven exciter are applied and compared; they are discussed below.

1. The effect can be simply simulated as a concentrated harmonic force. Its amplitude is then estimated as the product of the total mass of the exciter and its acceleration. To this end, a relative velocity amplitude of the exciter acting on the plate is measured, and from this result the acceleration amplitude of the exciter is calculated (by multiplying the velocity amplitude by angular frequency).
2. A more accurate approach assumes a weight-on-a-beam model (see, for example, Fig. 2, right) where the APA is modeled as a simple 3D beam with the excitation applied as a harmonic "initial" strain (using the thermoelastic analogy for the piezoelectric effect). The weight is precisely modeled as a 3D solid cylinder.

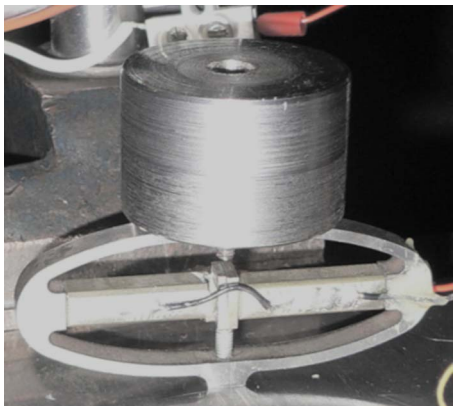

Fig. 7 Exciter

The first approach does not (directly) take into account the inertia of exciter. Nevertheless, as expected: Since the exciter is situated closely to the clamped area, this simplification is quite correct (that is, it does not affect significantly the relevant natural frequencies and modes). Moreover, the second (seemingly more accurate) approach requires modeling of the joint where the exciter is fixed to the plate and this may pose some difficulty.

4.4 Piezopatch Actuator. The single piezopatch actuator is mounted on the plate in the form of the following layers (see Fig. 8):

- a 0.1-mm-thick layer of epoxy resin (the assumed elastic modulus is 700 MPa)
- a 0.3-mm-thick aluminum tile
- a 0.1-mm-thick layer of epoxy resin
- a 0.3-mm-thick patch of piezoelectric material, Pz27 ceramic, with dimensions: $25\times5\ \mathrm{mm}^2$; the relevant material properties are as follows: the mass density is $7700\ \mathrm{kg}/\mathrm{m}^3$, the relevant elastic compliances are $[s_{11}, s_{33}]=[17, 23]\times10^{-12}\ \mathrm{m}^2/\mathrm{N}$, the relevant piezoelectric coefficients are $[d_{31}, d_{33}, d_{15}]=[-170, 425, 500]\times10^{-12}\ \mathrm{m}/\mathrm{V}$, and the relative dielectric constant equals 1800

The aluminum tile is used to facilitate the fixation of the wires to electrodes and the handling of the actuators (the piezoelectric patches are very brittle). The electrodes are situated on the opposite sides of piezoelectric patches so when an electric signal is sent to them any difference in the voltage between the two electrodes produces an electric field in the piezoelectric patch. The direction of the field is across the thickness of patch and its magnitude equals the electric potential difference divided by the thickness. The electric field developed in the piezoelectric material makes the (free) patch to expand or contract, and this expansion

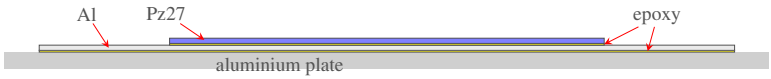

Fig. 8 Piezopatch actuator

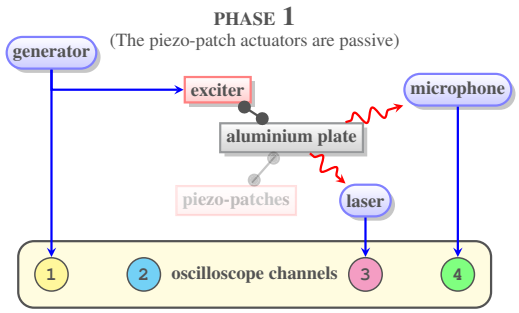

Fig. 9 Diagram of the phase 1 of experiment (passive behavior)

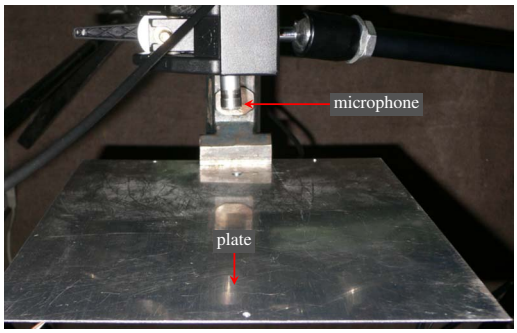

Fig. 11 A microphone behind the plate

and contraction can be controlled by changing the signal in time.

All the layers of actuator are thoroughly modeled using the finite element method accordingly with the displacement formulation of elasticity for the aluminum tile and the epoxy resin, and the mechanical-displacement-electric-voltage formulation of piezoelectricity for the ceramic piezopatch.

The piezopatch actuators are aimed to reduce these low-frequency vibration modes of plate, which may produce a significant low-frequency noise. Certainly, the feasibility and efficiency of that reduction depend among other things on the positioning of actuators on the plate surface.

5 Results of Modeling and Experimentation

5.1 Low-Frequency Noise Simulation. The first phase of experiment aims to simulate an annoying effect of low-frequency structure-borne noise. Thus, the piezopatch actuators are passive. An outline of this passive phase is depicted by the diagram in Fig. 9 and explained as follows (see also Fig. 4).

1. A harmonic signal of low-frequency (the chosen noisy frequency of panel: $f=115$ Hz) is sent by the generator to the exciter fixed on the elastic plate (and to the oscilloscope, where it can be observed).
2. The exciter induces significant vibrations of the plate.
3. In chosen points on the plate surface, the amplitude of velocity of the normal deflection of plate can be measured by the laser vibrometer (see Fig. 10) and observed on the oscilloscope.
4. The vibrating plate generates a low-frequency noise, which propagates in the air from both surfaces of the plate in the form of harmonic acoustic waves.
5. The noise, or more specifically, the amplitude of acoustic pressure, is measured by the microphone placed at some chosen distance from the plate (see Fig. 11); the measured signal is sent to the oscilloscope.

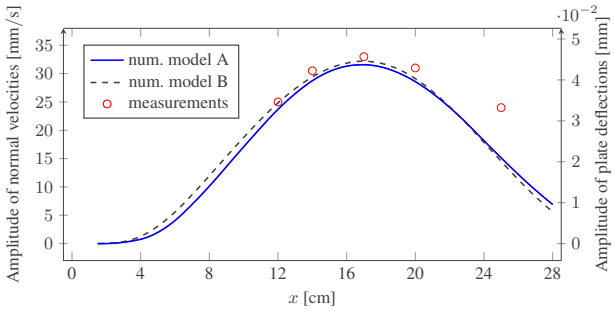

Fig. 10 Amplitude of normal velocities and deflections (along the line $y=0$ mm) of the plate with 6 passive piezopatch actuators (for harmonic excitation with frequency 115 Hz)

For simulation and optimization purposes, it is vital to possess an accurate model of this acoustic-structure interaction problem, that is, the model for which the computed amplitudes of the velocity of vibrations and acoustic pressure are very similar to the measured values. Such model has been described in Sec. 3 where the setting of boundary conditions have been discussed. The radius of the (quarter) sphere of surrounding air is assumed to 22 cm.

It seems obvious that a harmonic analysis of plate should be carried out for the chosen noisy frequency. However, one must remember that when approaching an eigenfrequency, the amplitudes of deflection increase and—in theory—they reach infinity at the very eigenfrequency. In reality, a system in the vicinity of its eigenfrequency, although manifests the increase, may still behave in a linear manner, although in the case of weakly damped systems when the eigenfrequency is being reached the assumption of small amplitudes of vibrations is often violated and the vibrations may become unstable. Thus, the frequency and the excitation amplitude assumed in the modeling should not only reflect the experimental data and assessment, but eventually they should produce a computed response, which is very similar to the measured one. If it is attainable, it means that the model is correct and accurate. The successive steps to check this are explained as follows. For further analysis, the stable frequency of 115 Hz is chosen, which produces the noisy vibrations in the shape of the fifth eigenmode. The amplitude of time-harmonic excitation force of frequency 115 Hz is estimated as 0.38 N. This is done according to the procedure described above in Sec. 4.3, which is based on the assessment of the amplitude of acceleration of the exciter acting on the plate. This estimation will be used for the concentrated force, which models the effect of the exciter. A similar assessment can be also used for the weight-on-a-beam model where the amplitude of time-harmonic "initial" strain is estimated as 0.00034 so that the resulting amplitude of weight's acceleration be similar as the measured value. (This estimated initial strain is applied for the 3D beam element simulating the APA100M actuator to which a bulky mass is fixed modeled as a solid cylinder.) The amplitudes of velocity of the deflection of plate are measured by the laser in different characteristic points on the plate surface, for example, at the (more and less maximal-deflection) point ($x=170$ mm, $y=0$ mm), it is approximately 33 mm/s.

Now, the estimated amplitude of force is used for the harmonic excitation (with the effect of the exciter simulated by a concentrated force), in numerical analysis where the frequency is chosen to 115 Hz and so that the amplitude of velocity of the deflection of plate at the point ($x=170$ mm, $y=0$ mm) should reach approximately 33 mm/s. Similarly, in the weight-on-a-beam model with the estimated time-harmonic "initial" strain, the frequency may be tuned up (yet still being close to 115 Hz) so that the amplitude of velocity of the maximal deflection reaches approximately 33 mm/s. Figure 10 shows the velocities of plate deflection along the $y=0$ mm line for two numerical models compared with measurements taken in few points on that line. The curve of model A

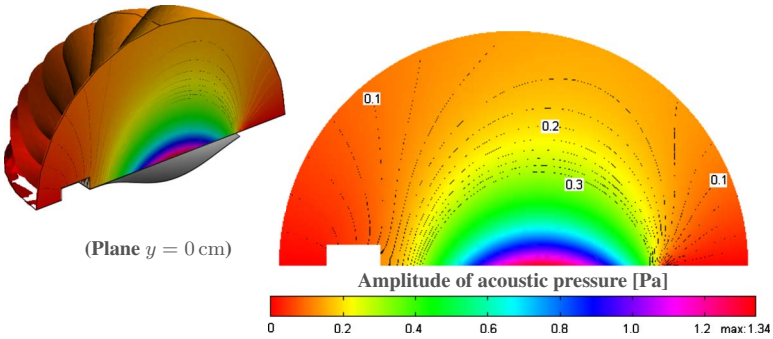

Fig. 12 Amplitude of acoustic pressure variation at plane $y=0$ cm obtained for time-harmonic excitation with frequency 115 Hz

presents the amplitudes of deflection velocities for the plate (excited with the concentrated force) with six passive, shunted piezopatches whereas curve B shows these amplitudes for the plate from the acoustic-structure interaction model. The curves agree very well and are in good accordance with the measured values.

The amplitude of acoustic pressure is measured by the microphone in different points behind the plate (see Fig. 11). The corresponding values computed from the numerical models (of acoustic-structure interaction) are in a very good accordance. For example, at the point ($x=170$ mm, $y=0$ mm, $z=40$ mm), the measured value is 0.31 Pa, and the computed one 0.33 Pa.

Figure 12 shows the acoustic pressure variation, calculated for the harmonic excitation of frequency 115 Hz, at plane $y=0$ cm, that is, the plane perpendicular to the plate, situated alongside its longer edges and passing through the center. In the case of symmetric modes, it is the very plane of symmetry used to reduce the numerical model. The biggest acoustic pressure occurs at the surface of plate close to the center where the amplitude reaches 1.34 Pa; however, just a few of centimeters from that point, it goes well below 0.5 Pa. The biggest amplitudes of acoustic pressure, which "propagate" outside the modeled sphere of air (of radius 22 cm), reach 0.15 Pa. To better illustrate the drop of acoustic pressure with increasing distance from the plate, Fig. 13 presents how the amplitude of acoustic pressure varies along a segment of the line defined by the intersection of planes $x=15$ cm and $y=0$ cm. Moreover, these results are compared with the measurements taken by the microphone successively placed in different points behind the plate; one should observe that the discrepancies between the measured and the computed values are very small indeed.

From the point of view of sound engineering, the acoustic pressure is not a very practical quantity. A much more useful quantity is the sound pressure level (SPL), which is a logarithmic scale defined as

$$\mathrm{SPL} = 10 \log_{10}\left(\frac{p_{\mathrm{rms}}^2}{p_{\mathrm{ref}}^2}\right) = 20 \log_{10}\left(\frac{p_{\mathrm{rms}}}{p_{\mathrm{ref}}}\right) \quad [\mathrm{dB}] \tag{20}$$

where

$$p_{\mathrm{rms}} = \sqrt{\frac{1}{t_{\mathrm{av}}}\int_0^{t_{\mathrm{av}}} p^2(t)\mathrm{d}t}, \quad p_{\mathrm{ref}} = 20 \ \mu\mathrm{Pa} \tag{21}$$

Here, p_{rms} is the root-mean-square pressure (computed for a time-variation of the acoustic pressure $p(t)$), and p_{ref} is the reference pressure; t_{av} is the averaging time. (For sinusoidal variation of $p(t)$ with amplitude A: $p_{\mathrm{rms}}=A/\sqrt{2}$.)

The isosurfaces of sound pressure level obtained for time-harmonic excitation with frequency 115 Hz are presented in Fig. 14. One should observe the following:

- At the plate surface (in the center), the SPL exceeds 96 dB.
- At approximately 15 cm from the center of plate, the SPL goes below 76 dB.
- There is, however, a large region (which extends much farther than 22 cm from the center of plate) where the SPL is still above 75 dB.

Notice eventually, that 20 or 30 cm is certainly a distance that occurs between an ear of a passenger in aircraft and the paneling of fuselage. Finally, Fig. 14 shows also the streamlines of fluid particle velocity (though their thickness and grayscale coloring correspond again to the SPL at the points of their pathway). One may notice that these streamlines are perpendicular to the isosurfaces. This is an obvious observation if one remembers that the gradient of acoustic pressure and the fluid velocity are linearly

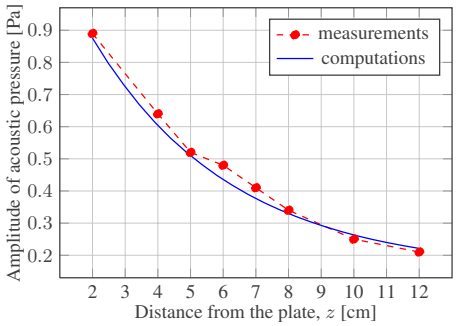

Fig. 13 Amplitude of acoustic pressure at line $x=15$ cm, $y=0$ cm (for harmonic excitation with frequency 115 Hz)

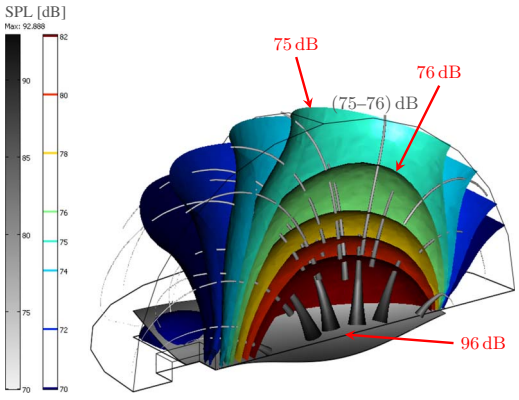

Fig. 14 Sound pressure levels (SPL) for time-harmonic excitation with frequency 115 Hz

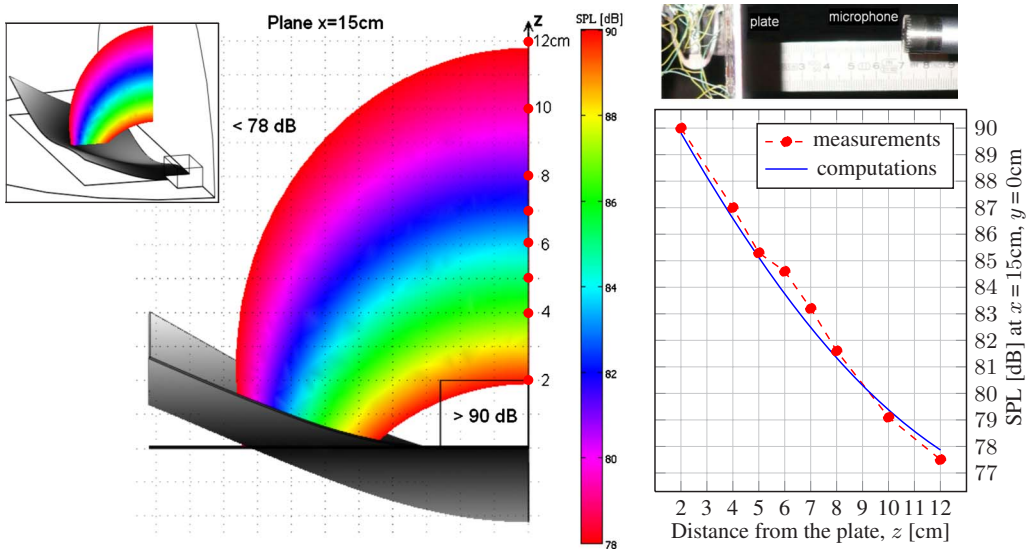

Fig. 15 SPL at the plane x=15 cm (the excitation frequency is 115 Hz)

related to each other, and that for time-harmonic problems the isosurfaces of SPL are also the isosurfaces of the amplitude of acoustic pressure (which is clearly seen from the definition of SPL).

Figure 15 shows the sound pressure level at plane $x=15$ cm. Now, one can clearly see that it can reach 90 dB at 2 cm from the plate surface, and at 12 cm it does not exceed 78 dB. These results are validated by the measurements taken by the microphone (and, independently, with the usage of a Bruel & Kjaer hand-held sound analyzer) in different points behind the plate: particularly, at some points on the line defined by the intersection of planes $x=15$ cm and $y=0$ cm. Again, the computed and measured results (see Fig. 15, right) are very much alike.

5.2 Active Reduction of Structure-Borne Noise. Figure 16 shows a schematic diagram of the second phase of experiment during which the active reduction of structure-borne noise is tested. The proceeding begins as in the first phase and thus the five steps listed in Sec. 5.1 remain valid: the plate is excited at low-frequency, the vibrations and the generated noise are measured (by the laser and the microphone, respectively). There is now, however, a vital difference: the piezopatch actuators are no longer passive; they become active as explained in the following.

6. The same harmonic signal, which is being sent to the exciter, is now also sent to a signal changer where it can be adjusted.
7. From the signal changer, the adjusted signal is sent to the electrodes of the piezopatch actuators, which begin to expand and contract harmonically, and that behavior locally affects the bending of the plate since the piezopatch actuators are glued to its surface.
8. The action of piezopatch actuators is aimed to reduce the noisy modes of vibration of the plate in order to reduce the generation of noise. The reductions are observed on the oscilloscope (thanks to the laser continuously measuring the vibrations, and the microphone continuously measuring the noise) and the observations can be used to better adjust the signal sent to the actuators.

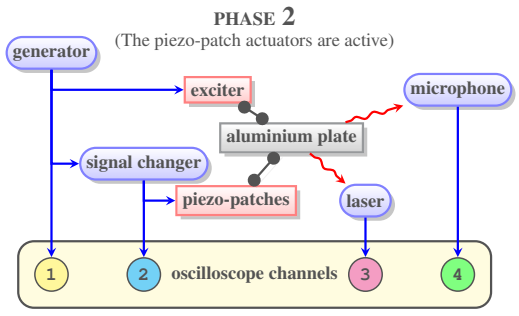

Fig. 16 Diagram of the phase 2 of experiment (active behavior)

The size of expansion and contraction of piezopatches, and consequently, the bending forces exerted on the plate depend on the amplitude of the signal sent to the electrodes. Here, the signal is simply a transformed signal of a known harmonic excitation, and the transformation can be carried into effect by a very simple signal changer (see Fig. 17). In practice, when the excitation is not known, the active reduction signal should be generated by an automatic control equipment based on the readings of some sensors, which can monitor the identified noisy modes of vibration (for example, piezoelectric sensors made up from PVDF foil and fixed in proper places to a faceplate of panel).

Figure 17 shows a schematic diagram of the fixed-frequency signal changer as well as its realization on a terminal plate. The signal changer can be simultaneously used to (1) shift the phase of the input signal and (2) change its voltage amplitude. The signal changer circuit is composed of two operational amplifiers, a capacitor, and several resistors (a few additional stabilizing capacitors that were also used are not shown on the scheme in Fig. 17). Each of the operational amplifiers is manually controlled by a potentiometer. Thus, one subcircuit permits to change the amplitude of the input signal, while the other one can be used to change its phase. One should also notice that the phase shift of 180 deg should be realized by fixing the wires to the proper electrodes of piezopatches (to change the phase by 180 degrees one needs only to connect the wires the other way round).

Several numerical tests of active reduction of structure-borne noise were carried out before the piezopatch actuators were actually glued to the plate. The tests allowed to choose an efficient placement of piezopatch actuators and check the feasibility of the active approach. Moreover, the voltage amplitudes for the active signal were correctly estimated during the numerical tests. The numerical tests involved one, two, and three pairs of symmetrically placed actuators. For example, Fig. 18 shows passive and

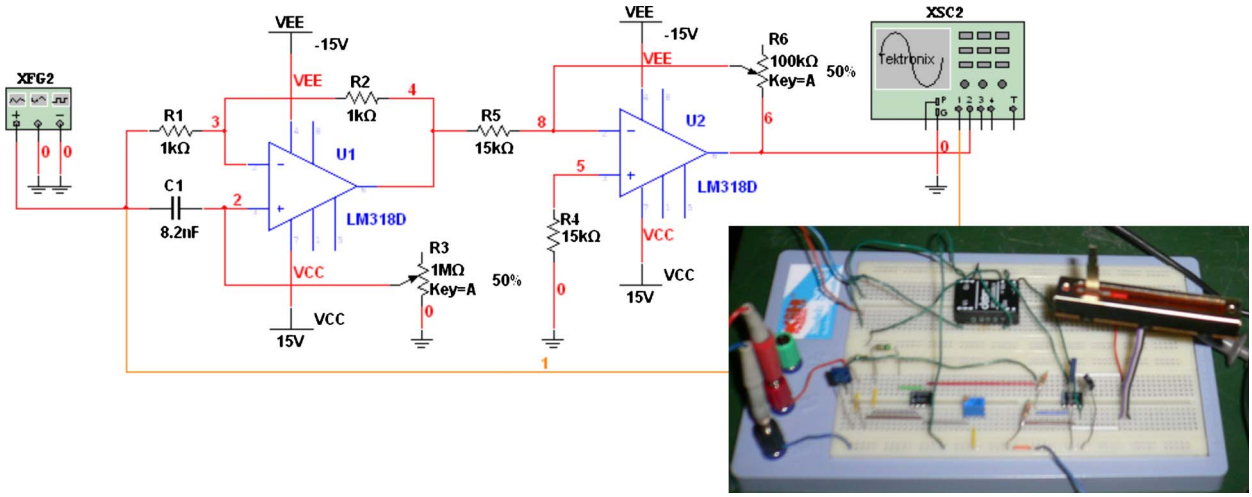

Fig. 17 Fixed-frequency signal changer

active behavior of the plate with only one pair of piezopatch actuators. During the passive behavior (when the piezopatch actuators are shorted) the plate—excited at the low-frequency of "loudspeaker" mode—undergoes free vibrations of significant amplitude (see Fig. 18, left), and becomes a dipole source of low-frequency noise (as it has been proven experimentally and by the numerical analysis of acoustics-structure interaction). This noisy behavior can be mitigated if a proper electric signal is sent to the piezopatch actuators, which, eventually, may result in an active behavior presented in Fig. 18 (right), where the same scale of deformation is used as in the passive case. It is clearly visible that such active behavior suppresses the emission of transmissible (i.e., low-frequency) noise. The same signal is sent simultaneously to the both actuators and the necessary peak-to-peak amplitude is found to be 43 V.

Finally, to efficiently deal with the loud-speaker mode, the three pairs of actuators are mounted at $x=130$, 145, and 160 mm from the clamped edge, approximately 25 mm from the x-axis on its both sides, with their length along the y-axis (see Fig. 5). The pair in the middle (at $x=145$ mm) was used in the analysis discussed above and illustrated by plots in Fig. 18. Another analysis, with two pairs of actuators (at $x=145$ and 130 mm) was carried out and showed that the necessary peak-to-peak amplitude can be thus decreased to 32 V (if the same signal is sent to all four actuators). The relevant plots are shown to the right sides of Figs. 19–21 (for a passive, active, and also an overload state—as discussed below). Very similar plots were also obtained from the analysis where all three pairs of actuators were involved. Obviously, this final analysis provided the smallest estimation of 20 V for the peak-to-peak amplitude of the control signal sent to the actuators.

Experimental tests were carried out, successively, for one, two (see Fig. 4), and three pairs of piezopatch actuators (see Fig. 5) glued to the surface of plate in the locations determined by the numerical tests. These experiments showed that the estimations for the amplitudes of control signal provided by the numerical tests are quite correct. Now, photographs in Figs. 19–21 present the results of experimental tests as read from the oscilloscope. The readings show signals from four channels (see also the diagram in Fig. 16):

- channel 1 (CH1, yellow curve in the middle)—the signal produced by the generator and sent to the exciter
- channel 2 (CH2, cyan curve in the middle)—the modified signal sent by the signal changer to the piezopatch actuators

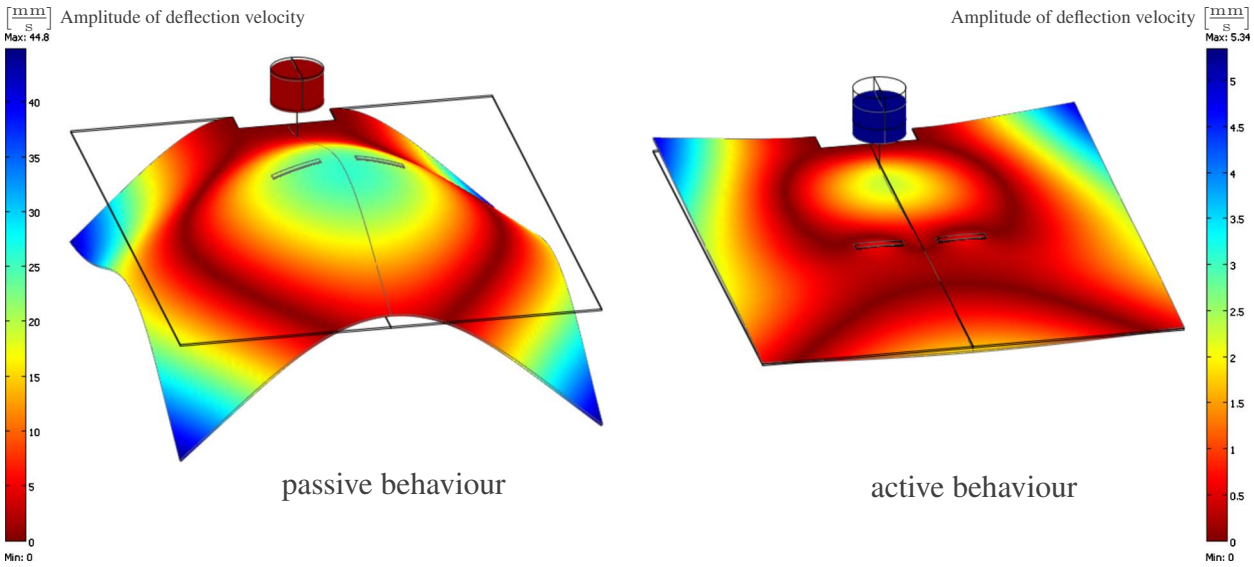

Fig. 18 Passive and active behavior of plate

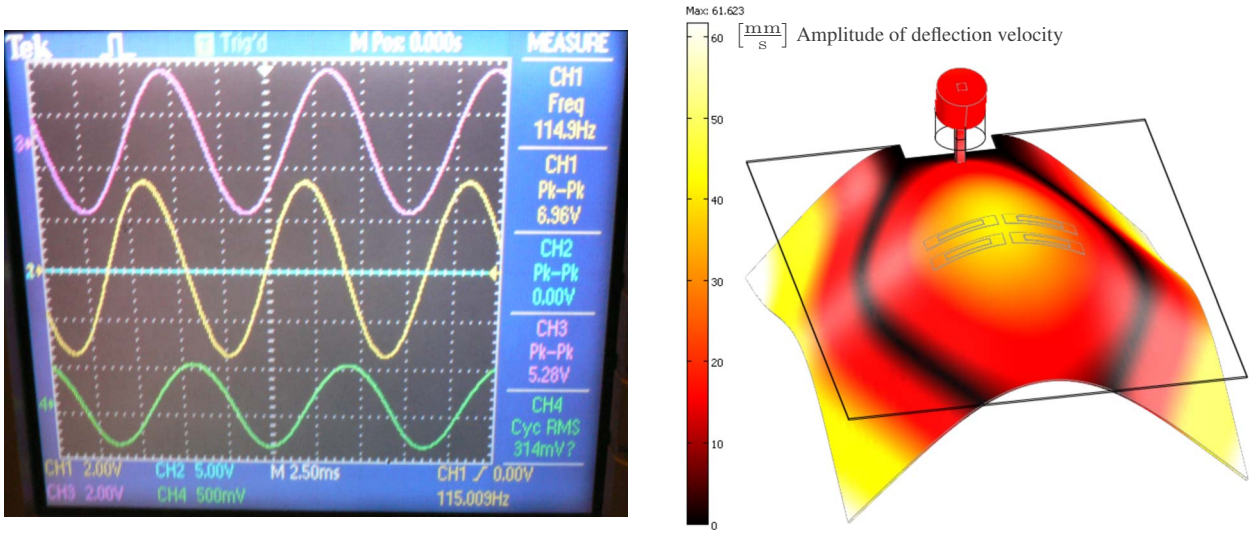

Fig. 19 The "noisy behavior" of plate with passive piezopatch actuators

- channel 3 (CH3, magenta curve at the top)—the vibrations measured by the laser vibrometer
- channel 4 (CH4, green curve at the bottom)—the noise measured by the microphone

The signal sent to the exciter was a harmonic of frequency 115 Hz. The laser vibrometer measured the deflection velocities at a central point on the plate ($x=170$ mm), and the microphone was situated approximately 6 cm behind the plate.

A "noisy behavior" of panel is shown in Fig. 19. The electrodes of piezoelectric patches are shorted (thus, the corresponding curve on the oscilloscope is a straight line of 0 V), and so the actuators are passive. The plate driven by the exciter freely vibrates and emits a significant low-frequency noise. The amplitude of acoustic pressure (registered at the point of measurement by the microphone) is 0.22 Pa.

Figure 20 shows an experimental verification of the active reduction of structure-borne noise. Now, the harmonic signal of the peak-to-peak amplitude of approximately 23 V is applied to the electrodes of piezopatch actuators. Such amplitude is chosen in order to damp the noisy mode of vibration; it is slightly bigger than 20 V, estimated numerically (similar discrepancies between the simulation and experimental results were observed by Malgaca and Karagülle [11] in their active vibration control of smart beams under harmonic excitation). Now, the amplitude of plate deflections is less than 5% of the original (undamped) value, and the noise is no longer audible. The shape of vibrations is significantly different from the undamped one (see Fig. 19), and as a source of sound it is not so efficient. Moreover, the amplitudes of deflection are now much smaller, especially, at the center of the plate (notice that the plots in Figs. 19 and 20 have the same scale of deformation). The reduction of noise—assessed based on the amplitudes of acoustic pressure registered by the microphone—is very big indeed and reaches 97% (based on a logarithmic scale such as SPL—it means 36% reduction).

Finally, Fig. 21 shows a case when an overload signal is sent to the electrodes of piezoelectric patches: the peak-to-peak amplitude of 27 V is too big. Since the signal is too strong, the countervibrations caused by the piezopatch actuators are significant (the amplitude of deflection is nearly 17% of the amplitude of undamped vibrations). Thus, a noise is audible again, although it is quieter than the noise of the passive phase. The microphone measurements permit to estimate it for nearly 20% of the un-

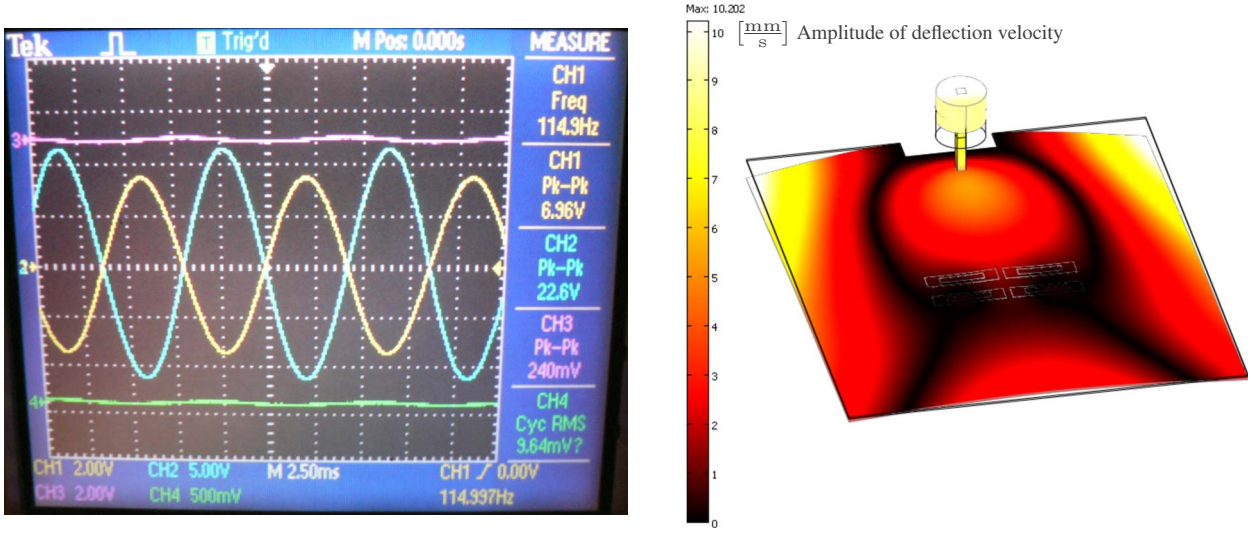

Fig. 20 Active reduction of structure-borne noise

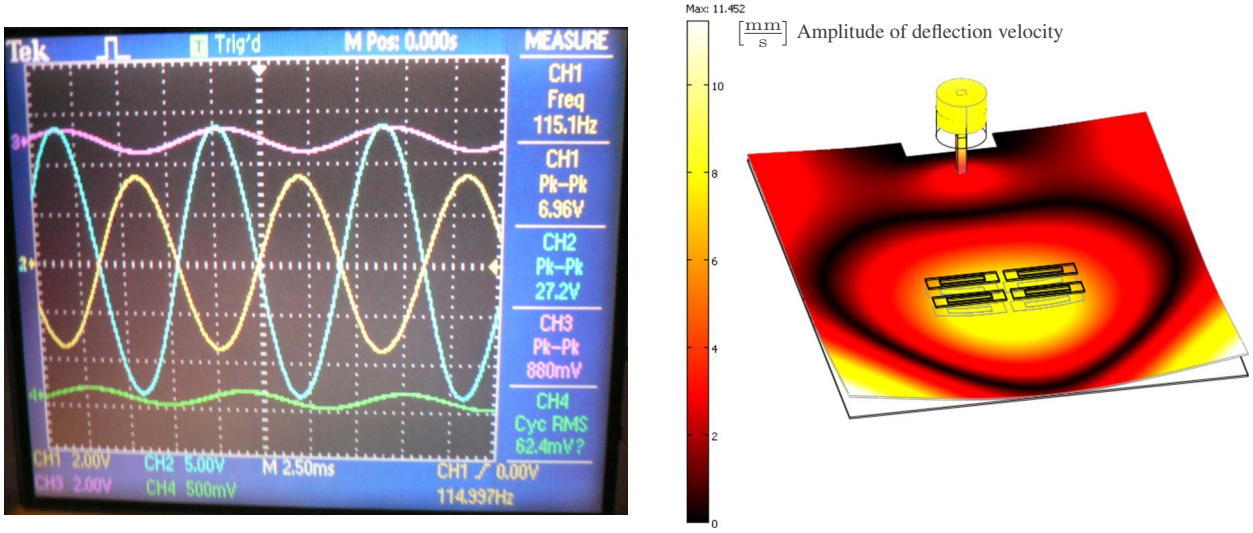

Fig. 21 Generation of noise by overloaded piezopatch actuators

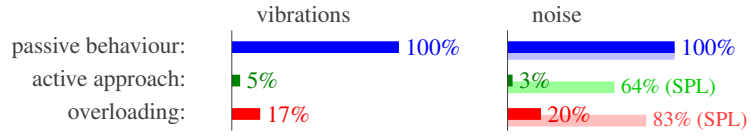

Behaviour	Control voltage [V]	Vibr. amp. at ($x = 17$ cm, $y = 0$ cm) vel. [mm/s]	defl. [mm]	rel. [%]	Noise at ($x = 17$ cm, $y = 0$ cm, $z = 6$ cm) p_{amp} [Pa]	p_{rms} [Pa]	rel. [%]	SPL [dB]	rel. [%]
passive:	0	33.0	0.0457	**100**	0.444	0.314	**100**	83.9	**100**
active:	22.6	1.5	0.0021	**5**	0.014	0.010	**3**	53.7	**64**
overloading:	27.2	5.5	0.0076	**17**	0.088	0.062	**20**	69.9	**83**

Fig. 22 Quantitative results of experimental tests

damped noise, so with such moderate overloading one can still experience a very significant reduction of noise by 80% (it means 17% reduction of SPL).

6 Conclusions and Further Investigations

The combined quantitative results of experimental tests are shown in Fig. 22, where the vibrations and noise measured during the active phase (both for the proper controlling signal and for the overloaded one) are presented relatively to the measurements from the passive phase; compared are the amplitudes of deflection (for vibrations) and the amplitudes of acoustic pressure (for noise). Additionally, in the case of noise, the relative change in logarithmic scale (SPL) is also given. It is clear that the chosen setup of piezopatch actuators allows for an almost complete reduction of the noise generated by the noisy low-frequency mode of vibrations (at approximately 115 Hz). However, an efficient control system is necessary to prevent overloading and deal with the noise emitted by multifrequency and/or pulsing vibrations.

The presented multiphysics approach enabled an effective choice of shape and localization for the piezopatch actuators, and—at the same time—to check the feasibility of the active reduction of structure-borne noise. A similar analysis should be extremely useful when developing a control system of high efficiency. Such control system should use a set of sensors in order to check whether a low-frequency noise is being generated and to assess its volume. As a matter of fact, the assessment of noise may be indirect in that way that the sensors should simply measure some deflections of the panel's surface and not, for example, the acoustic pressure close to the surface. Thus, instead of microphones, simple sensors made up from, for example, a PVDF foil could be used. The measurements should allow to establish if and what noisy modes of low-frequency are induced. Therefore, the noisy modes should be first identified numerically and—possibly—also experimentally (like it has been shown in this paper). Then, another multiphysics analysis should be carried out in order to design the shape and localization of the sensors.

As it has been stated at the beginning of this paper, the noise generated by higher frequency vibrations should be passively reduced (or not transmitted at all) by acoustically isolating layers of very moderate thickness and weight. Such layer or layers form a lightweight core of panel. They are usually porous materials of rather high porosity. If the structural strength of the whole panel is important, a stiff periodic composites—like honeycomb structure—are often used. Eventually, thin elastic structures may be embedded inside the core in order to increase even more the stiffness of panel, and possibly, also to improve its (passive) acoustic insulation in the medium frequency range, although this latter effect may prove opposite if not taken care of during design. Moreover, it is worthwhile investigating if some of these embedded elements could be piezoelectric and actively controlled to improve the acoustic absorption and/or transmission loss in the low-frequency range. Still, the piezoelectric actuators can be also situated on the faceplates. In order to design and test such active composites, a multiphysics analysis, similar to the one presented here, yet involving an advanced (possibly, biphasic) modeling of the acoustic wave propagation in porous or periodic media would be necessary.

Acknowledgment

Financial support of the Foundation for Polish Science Team Programme, cofinanced by the EU European Regional Develop-

ment Fund Operational Programme "Innovative Economy 2007–2013:" Project "Smart Technologies for Safety Engineering—SMART and SAFE," Grant No. TEAM/2008-1/4, and Project "Modern Material Technologies in Aerospace Industry," Grant No. POIG.0101.02-00-015/08, is gratefully acknowledged.

References

[1] Fuller, C. R., Elliott, S. J., and Nelson, P. A., 1996, *Active Control of Vibration*, Academic, New York.
[2] Nelson, P. A., and Elliott, S. J., 1992, *Active Control of Sound*, Academic, New York.
[3] Fahy, F. J., and Gardonio, P., 2007, *Sound and Structural Vibration: Radiation, Transmission and Response*, 2nd ed., Academic, New York.
[4] Fuller, C. R., 1990, "Active Control of Sound Transmission/Radiation From Elastic Plates by Vibration Inputs. Part I: Analysis," J. Sound Vib., **136**, pp. 1–15.
[5] Metcalf, V. L., Fuller, C. R., Silcox, R. J., and Brown, D. E., 1992, "Active Control of Sound Transmission/Radiation From Elastic Plates by Vibration Inputs. Part II: Experiments," J. Sound Vib., **153**, pp. 387–402.
[6] Lin, Q., Liu, Z., and Wang, Q., 2001, "Active Control of Structural Acoustic Pressure in a Rectangular Cavity Using Piezoelectric Actuators," Eur. J. Mech. A/Solids, **20**, pp. 573–583.
[7] Li, S., and Zhao, D., 2004, "Numerical Simulation of Active Control of Structural Vibration and Acoustic Radiation of a Fluid-Loaded Laminated Plate," J. Sound Vib., **272**, pp. 109–124.
[8] Choi, S.-B., 2006, "Active Structural Acoustic Control of a Smart Plate Featuring Piezoelectric Actuators," J. Sound Vib., **294**, pp. 421–429.
[9] Carneal, J. P., and Fuller, C. R., 2004, "An Analytical and Experimental Investigation of Active Structural Acoustic Control of Noise Transmission Through Double Panel Systems," J. Sound Vib., **272**, pp. 749–771.
[10] Ray, M. C., and Balaji, R., 2007, "Active Structural-Acoustic Control of Laminated Cylindrical Panels Using Smart Damping Treatment," Int. J. Mech. Sci., **49**, pp. 1001–1017.
[11] Malgaca, L., and Karagülle, H., 2009, "Simulation and Experimental Analysis of Active Vibration Control of Smart Beams Under Harmonic Excitation," Smart Struct. Syst., **5**(1), pp. 55–68.
[12] Zielinski, T. G., Galland, M.-A., and Ichchou, M. N., 2005. "Active Reduction of Vibroacoustic Transmission Using Elasto-Poroelastic Sandwich Panels and Piezoelectric Materials," Proceedings of Symposium on the Acoustics of Poro-Elastic Materials SAPEM'05, Lyon, France.
[13] Zielinski, T. G., Galland, M.-A., and Ichchou, M. N., 2006, "Further Modeling and New Results of Active Noise Reduction Using Elasto-Poroelastic Panels," Conference Proceedings of ISMA2006, Leuven, Belgium.
[14] Batifol, C., Zielinski, T. G., Ichchou, M. N., and Galland, M.-A., 2007, "A Finite-Element Study of a Piezoelectric/Poroelastic Sound Package Concept," Smart Mater. Struct., **16**, pp. 168–177.
[15] Filipek, R., and Wiciak, J., 2008, "Active and Passive Structural Acoustic Control of the Smart Beam," Eur. Phys. J. Spec. Top., **154**, pp. 57–63.
[16] Benjeddou, A., 2000, "Advances in Piezoelectric Finite Element Modeling of Adaptive Structural Elements: A Survey," Comput. Struct., **76**, pp. 347–363.